Sheng Chen
Department of Mechanical Engineering,
Michigan State University,
East Lansing, MI 48824;
Department of Biomedical Engineering,
Michigan State University,
East Lansing, MI 48824
e-mail: chensh38@msu.edu

Megan R. Routzong
Department of Bioengineering,
University of Pittsburgh,
Pittsburgh, PA 15260
e-mail: mer136@pitt.edu

Steven D. Abramowitch
Department of Bioengineering,
University of Pittsburgh,
Pittsburgh, PA 15260
e-mail: sdast9@pitt.edu

Michele J. Grimm[1]
Department of Mechanical Engineering,
Michigan State University,
East Lansing, MI 48824;
Department of Biomedical Engineering,
Michigan State University,
East Lansing, MI 48824
e-mail: mgrimm@msu.edu

A Computational Procedure to Derive the Curve of Carus for Childbirth Computational Modeling

Computational modeling serves an important role in childbirth-related research. Prescribed fetal descent trajectory is a key characteristic in childbirth simulations. Two major types of fully prescribed fetal descent trajectories can be identified in the literature: straight descent trajectories and curve of Carus. The straight descent trajectory has the advantage of being simpler and can serve as a reasonable approximation for relatively small fetal movements during labor, but it cannot be used to simulate the entire childbirth process. The curve of Carus is the well-recognized fetal descent trajectory with physiological significance. However, no detailed procedure to geometrically define the curve of Carus can be found in existing computational studies. This status of curve of Carus simulation in the literature hinders the direct comparison of results across different studies and the advancement of computational techniques built upon previous research. The goals of this study are: (1) propose a universal approach to derive the curve of Carus for the second stage of labor, from the point when the fetal head engages the pelvis to the point when the fetal head is fully delivered; and (2) demonstrate its utility when considering various fetal head sizes. The current study provides a detailed formulation of the curve of Carus, considering geometries of both the mother and the fetus. The maternal geometries were obtained from MRI data, and the fetal head geometries were based on laser scanning of a replica of a real fetal head. [DOI: 10.1115/1.4055108]

Keywords: childbirth, computational modeling, fetal descent trajectory, curve of Carus

1 Introduction

Childbirth is a complex and physically intense biomechanical process during which both the mother and the child are under risk of injury. Common injuries to the mother include damage to the pelvic floor and perineum [1]. For the infants, common injuries related to childbirth include bony fractures, small vessel hemorrhages, hematomas, and nerve injuries [2]. Researchers and clinicians have explored multiple approaches, including retrospective data analysis, physical models, and computational models, to investigate mechanisms of childbirth-related injuries. Among different approaches, computational modeling has emerged as a powerful tool due to its unique characteristics and advantages. Computational models can help investigate issues that cannot be easily or ethically studied in a clinical setting. Compared to physical models, computational models have the advantage of allowing easy adaptation to subject-specific data and construction of a sophisticated biomechanical environment at higher precision and lower cost. In addition, computational models can help researchers control variables in a complex scenario and identify causative factors in a more reliable manner. By comparison, statistical analysis of retrospective observational data can identify risk factors but struggle to determine causative factors [3].

Computational models have been widely used by researchers to investigate childbirth-related topics. Stretch and stress analysis of the maternal pelvic floor soft tissues during childbirth is one of the most studied topics by computational models [4–8], due to their relevance to postpartum pain from the pelvic floor in the short term and potential pelvic organ prolapse in the long term [9]. With respect to fetal injuries, operative delivery (i.e., forceps delivery and vacuum delivery) induced injuries on the fetal head have been probed using numerical models [10,11], thanks to the excellent ability of variable-control by computational approaches. Mechanisms of complex injuries, like neonatal brachial plexus palsy, can be investigated due to computational models' efficiency and precision in building fetal articulations [12,13]. Besides injury mechanisms, topics like protective measures during labor [14,15] and childbirth characteristics (e.g., delivery force [16], fetal head flexion [17]) also benefit greatly from computational methods.

A key component of childbirth computational modeling is simulating the passage of the fetus through the maternal pelvis. There are two major approaches to driving fetal movements in computational models: (1) force-driven fetal movements; and (2) displacement-driven fetal movements. Force-driven models better match the physiology of childbirth, since uterine pressure is the direct driving force of childbirth [18–20]. However, for a force-driven model to accurately simulate the whole childbirth process, relatively complete maternal soft tissues (birth canal, pelvic floor, internal organs, etc.) should be present to provide boundary conditions for the fetal pathway. The presence of complete maternal soft tissues in a computational model requires a large amount of three-dimensional (3D) geometrical data and complicated contact conditions between each soft tissue group. This high demand for computational resources could be a major reason that force-driven childbirth computational models are rare in the literature. Displacement-driven fetal movement grants precise control over the descent trajectory without requiring the presence of complete maternal soft tissues. Displacement-driven fetal movement provides an easier yet more reliable alternative to force-driven fetal movements, which contributes to the more prevalent usage of the former approach. Two types of prescribed descent trajectories can be found in the literature: straight descent trajectory and curve of Carus. Straight descent trajectory, which is a straight pathway between its starting and ending points, is a reasonable approximation when only small movements of the fetus are involved (e.g., [6,8,17]). But a straight descent trajectory does not accurately

[1]Corresponding author.
Manuscript received December 14, 2021; final manuscript received July 18, 2022; published online August 19, 2022. Assoc. Editor: Nicole Hashemi.

describe movement of the fetal body during the entire second stage of labor. Some studies have tried to improve the accuracy of fetal head movement during a straight descent trajectory by allowing movements and rotations of the fetal head in directions other than the prescribed direction of motion (e.g., [21–28]). The curve of Carus is a widely accepted descent trajectory of the fetus with physiological significance and has been used in a number of computational models (e.g., [4,14,15,29,30]).

The curve of Carus was first defined by Carl Gustav Carus in the early 19th century [31], and it was described based on the connection of the various diameters of the planes of the pelvis. The curve results from the passive interaction of the fetus with the irregular structure of the mother's pelvis. In addition to the two-dimensional movement in the sagittal plane that is idealized by the curve of Carus, the interaction of the fetus and pelvis in three dimensions drives the cardinal movements of labor due to rotation of the infant's head about the axis of its neck as well as in flexion and extension [32].

However, no detailed procedure to determine the curve of Carus within a computational model is provided in the papers that utilized a descent trajectory based on this curve. This makes it difficult to compare results from different studies and hinders researchers who are trying to reproduce models in the literature. The goal of the current study is to propose a detailed procedure to geometrically define the curve of Carus that can be applied to any fetal head and maternal pelvis geometries. The use of the curve is demonstrated when considering fetal heads of different sizes.

2 Method

A set of 3D computational models, including a maternal pelvis and a series of fetal heads of different sizes, was developed. The maternal geometric model was based on the in vivo MR images of a 21-year-old nulliparous woman at the gestational stage of 35 weeks and 6 days, collected retrospectively with Institutional Review Board approval. The 3D maternal geometric model included both innominate bones, the sacrum, and the pubic symphysis of the bony pelvis, excluding the coccyx (Fig. 1). The pelvic model was discretized using shell elements of 5 mm size and 1 mm thickness.

The fetal head model was based on the laser scanning of an exact replica of a real fetal skull model, as shown in Lapeer and Prager [33] (Figs. 2(*a*) and 2(*b*)). This fetal skull model was then scaled to match the 50th percentile size of the fetal head at 40 weeks using measurements of biparietal and occipito-frontal diameters reported by Chitty et al. [34] A fetal mandible was developed using the mean measurements (i.e., height of the ramus, length of the body of the mandible, and sagittal length) at 40 weeks [35]. A smooth surface was then created to wrap the fetal skull and the fetal mandible to form the fetal head model (Figs. 2(*c*) and 2(*d*)). This 40-week, 50th percentile sized fetal head model was scaled down to match the size of the 10th percentile and up to match the 90th percentile sized fetal heads at 37 weeks of gestational age, using the measurements of biparietal diameter and occipito-frontal diameter [34]. 37-week gestational age was selected so that the fetal head was for a full-term infant, while the fetal head sizes at the 10th, 50th, and 90th percentile were able to move through the pelvis without allowing for molding. The fetal head models were discretized using shell elements of 4 mm size and 1 mm thickness.

The maternal pelvis was positioned with a 45 deg angle between the long axis of the pubic symphysis and the X-Y plane, to simulate a lithotomy childbirth position. The descent trajectory of the fetal head during childbirth followed the curve of Carus. It passed five landmark points (Fig. 3(*a*)) described as follows—P_1: the middle point of the pelvic inlet, which is from the proximal end of the pubic symphysis to the proximal end of the sacrum; P_2: the middle point of the midpelvic cavity, which is from the middle of the pubic symphysis to the middle of the sacrum (the third sacral vertebrate); P_3: the middle point of pelvic outlet, which is from the distal end of the pubic symphysis to the distal end of the sacrum; P_4: the closest point to the pubic symphysis on the plane of the pubic arch that allowed the passage of the fetal head; and P_5: a point where the fetal head is fully delivered, with consideration of the anatomy of the vaginal soft tissues that were not included in the current study. The angle between the P_4–P_5 line and the X-Y plane was 45 deg, so that the P_4–P_5 line is perpendicular to the long axis of the pubic symphysis.

To obtain the location of P_4, the geometric relationship between the fetal head and the plane of the pubic arch was generalized, as shown in Fig. 3(*b*). Point A was the lowest point of the pubic symphysis. Points B and C were the forwardmost points at the junction areas between the inferior pubic rami and ischial rami. For this specific calculation, the fetal head geometry was simplified as a sphere with the diameter ($\overline{P_4D} \times 2$) equal to the biparietal diameter. The inferior pubic rami were simplified as two straight lines (AB and AC). While passing through the pubic arch, the fetal head will stay close to the pubic rami, due to the pressure from the pelvic floor and other surrounding maternal tissues. Therefore, AB and AC were tangents of the fetal head during the passage. An extra clearance of 2 mm was added in addition to the fetal head radius (half of the biparietal diameter) to form the length $\overline{P_4D}$, so that there was enough room for maternal soft tissues (when they are modeled) between the fetal head and the maternal pubic rami and to ensure the convergence of the MADYMO model. The coordinates of P_4 were determined through the following procedure:

(1) Subpubic angle α was obtained by calculating the angle between vector $\overrightarrow{AB}$ and vector $\overrightarrow{AC}$.
(2) The distance from P_4 to A was obtained from $\overline{P_4A} = \frac{\overline{P_4D}}{\sin\left(\frac{\alpha}{2}\right)}$. P_4 coordinates (x, y, z) were obtained by solving the following two equations

$$mx + ny + pz + q = 0 \tag{1}$$

$$\sqrt{(x - x_A)^2 + (y - y_A)^2 + (z - z_A)^2} = \overline{P_4A} \tag{2}$$

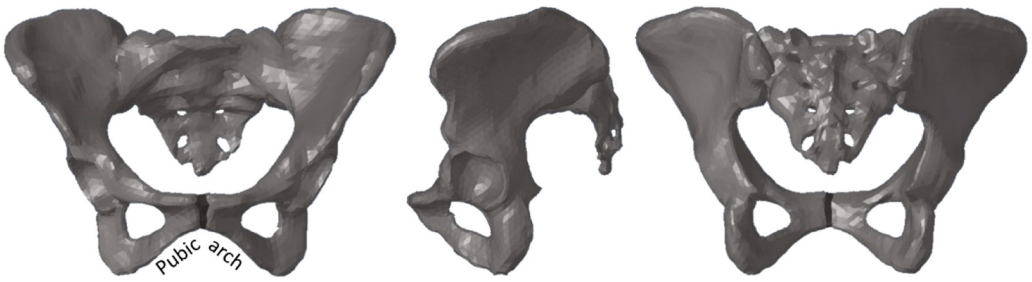

Fig. 1 The anterior view, left lateral view, and posterior view of a maternal pelvis model (sacrum and innominate bones) based on in vivo MR images of a 21-year-old nulliparous woman at the gestational stage of 35 weeks and 6 days

Equation (1) describes P_4 being on the pubic arch plane ABC, and Eq. (2) describes $\overline{P_4A}$ being known. The constants m, n, p, and q of plane ABC are found based on known coordinates of Points A, B, and C. In addition, $y = y_A$, due to P_4 and A both being on the midsagittal plane. The only two unknown variables, x and y, can then be calculated from Eqs. (1) and (2). After the P_4 coordinates are obtained, the P_5 position, which ensures the full delivery of the fetal head, can be determined.

After coordinates of all of the landmark points were determined, a cubic spline interpolation method provided by the MATLAB function *spline* was used to interpolate data between each pair of successive landmark points. The *spline* function provides piecewise cubic polynomial interpolants and ensures the continuous first and second-order derivative. The corresponding polynomial equation for each interval is as follows:

$$z = a(x - x_{P_n})^3 + b(x - x_{P_n})^2 + c(x - x_{P_n}) + d \tag{3}$$

where x and z are the x-coordinate and z-coordinate of points on the curve of Carus. For the P_1P_2 interval, $x_{p_n} = x_{P_1}$—namely, the x-coordinate of P_1. Similarly, for the P_2P_3 interval, $x_{p_n} = x_{P_2}$ (the x-coordinate of P_2); for the P_3P_4 interval, $x_{p_n} = x_{P_3}$ (the x-coordinate of P_3); and for the P_4P_5 interval, $x_{p_n} = x_{P_4}$ (the x-coordinate of P_4). Coefficients a, b, c, and d for each interval are achieved through the *spline* function, based on coordinates of P_1 through P_5.

The whole procedure can be summarized as follows: (1) find the pelvic cavity midpoints to determine P_1, P_2, and P_3, as shown in Fig. 3(*a*); (2) use Eqs. (1) and (2) to determine P_4, with the geometric relationship shown in Fig. 3(*b*); and (3) determine P_5 based on the angle between P_4P_5 and plane X-Y being 45 deg and the length of P_4P_5, ensuring full delivery of the fetal head.

The childbirth process was simulated in MADYMO (Siemens, version 2021.1), using the solver's finite element capabilities during a simulated time span of 3600 s. The fetal head moved along the curve of Carus at a constant speed. The starting position of the fetal head simulated a left occipito-transverse position (biparietal axis parallel to the Z-axis), with the flexed fetal head engaging the birth canal using its smallest diameter, namely, the suboccipitobregmatic diameter. This fetal head posture was simulated through the following criteria: (1) the midpoint of the suboccipitobregmatic diameter of the fetal head was placed at P1, and the midpoint of the suboccipitobregmatic diameter of fetal head followed the curve of Carus as labor proceeded; (2) the biparietal diameter of the fetal head was parallel to the plane of the pelvic inlet; and (3) the suboccipitobregmatic diameter was perpendicular to the maternal midsagittal plane. Rotational movements during labor were prescribed as well, based on the cardinal movements of labor. The fetal head rotated 90 deg along its longitudinal axis (ζ axis, as shown in Fig. 4(*a*)) from the occipito-transverse position to an occipito-anterior position when it moved from P_1 to P_4. This represents the internal rotation phase of the cardinal movements. To ensure that the fetal head engaged the birth canal using its smallest diameter (suboccipitobregmatic diameter) throughout labor, namely, with a posture of the head being flexed and the chin being against the chest, the fetal head rotated along its transverse axis (ξ axis, as shown in Fig. 4(*a*)) to keep the suboccipitobregmatic diameter parallel to the pelvic inlet plane, midpelvic cavity plane, pelvic outlet plane, and the pubic arch plane when the fetal head passed P_1, P_2, P_3, and P_4, respectively. The fetal head is eventually delivered at P_5, at which point it would normally experience external rotation – also known as restitution. Extension, which occurs before external rotation, was not modeled within the current paper.

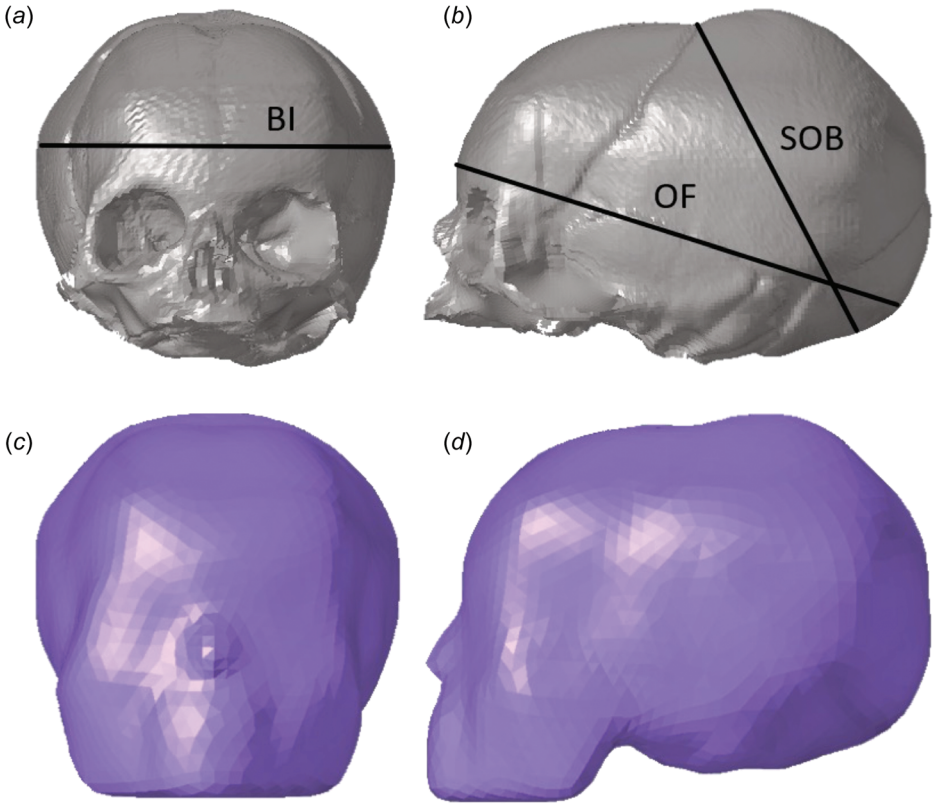

Fig. 2 The upper row shows the anterior view (*a*) and left lateral view, (*b*) of the laser scanning of the replica of a real fetal skull model [28]. The fetal head measurements shown in the picture are biparietal diameter (BI), suboccipitofrontal diameter (SOB), and occipito-frontal diameter (OF). The lower row shows the anterior view (*c*) and left lateral view (*d*) of the fetal head model with the added fetal mandible.

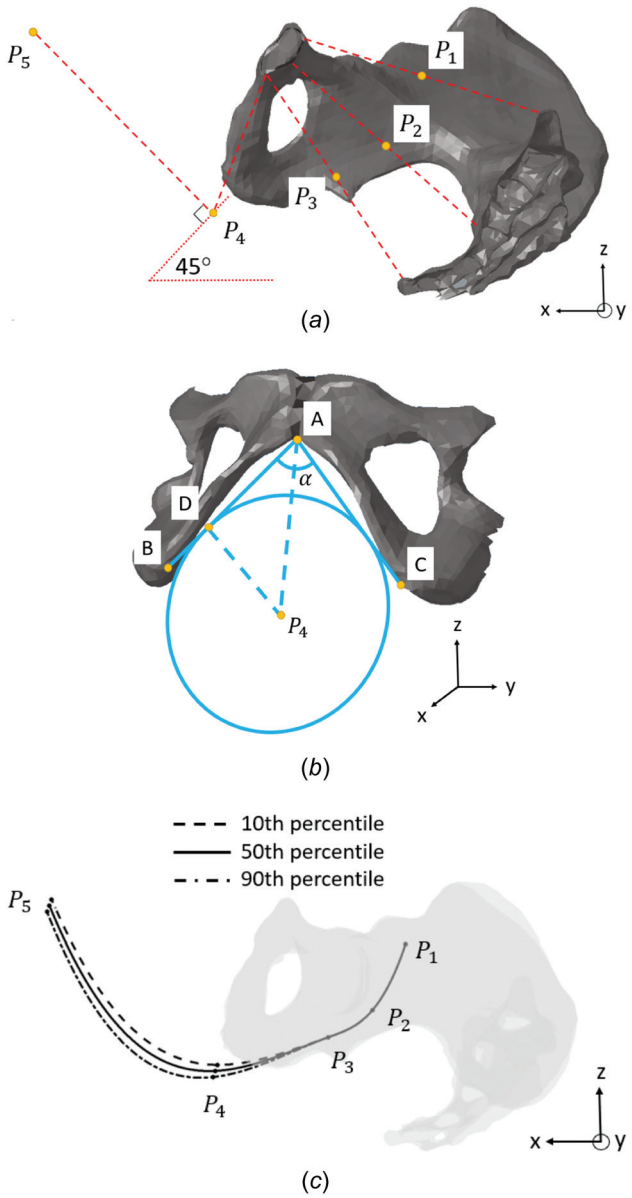

Fig. 3 (*a*) Five landmark points P_1–P_5 on the curve of Carus, with a midsagittal view of the maternal pelvis. (*b*) The geometric relationship between the fetal head and the pubic arch plane while the midpoint of the suboccipitobregmatic diameter of the fetal head is at point P_4. Point *A* is the lowest point of the pubic symphysis. Points *B* and *C* are the forwardmost points at the junction areas between the inferior pubic rami and the ischial rami. Point *D* is the tangent point between segment *AB* and a circle centered at P_4, and segment P_4D is perpendicular to segment *AB*. α is the angle between *AB* and *AC*. Note that the perspective for (*b*) has rotated the plane of the circle that represents the fetal head (yz-plane) slightly (i.e., the x-axis is not perpendicular to the page). (*c*) Three curves of Carus for the 10th, 50th, and 90th percentile fetal head sizes at 37 weeks, with a midsagittal view of the maternal pelvis.

3 Results

The measurements of the 10th, 50th, and 90th percentile-sized fetal heads at 37 weeks gestational age are listed in Table 1, along with other fetal head sizes from childbirth computational models in the literature.

The process of calculating the P_4 coordinates based on the geometric relationship between the maternal pubic arch plane and the fetal head size is shown in Fig. 5. Coordinates of key points *A*, *B*, *C* on the maternal pelvis are listed. The 50th percentile fetal head size at 37 weeks was used for the values provided in Fig. 5. Coordinates of landmark points P_1 to P_5 on the curve of Carus for the three fetal head sizes are listed in Table 2. As shown in Fig. 3(*c*), P_1, P_2, and P_3 remain the same for all three fetal head sizes since their locations are solely based on maternal pelvic geometries. P_4 coordinates are different for the three fetal head sizes: larger fetal heads result in P_4 being at a more posterior location, which is as expected based on the geometries shown in Fig. 3(*b*).

After the coordinates of P_1 to P_5 were determined, polynomial function coefficients *a*, *b*, *c*, *d* for each interval between two adjacent landmark points for different fetal head sizes were obtained and are listed in Table 3. It is worth noting that although P_1, P_2, and P_3 are the same for the three different trajectories of different fetal head sizes, sections P_1P_2 and P_2P_3 are not the same for the different fetal head sizes, which is demonstrated by the different coefficient values of *a*, *b*, *c*, and *d*. This is because *spline* function ensures the continuous first and second-order derivative of the entire trajectory. Therefore, different P_4 and P_5 locations would affect the shape of P_1P_2 and P_2P_3.

After the equation of the curve of Carus is obtained, the childbirth process can be simulated. Figure 4 shows the position and posture of the fetal head (50th percentile size at 37 weeks) at each of the landmark points. The fetal head starts engagement with the pelvic inlet at P_1 with a flexed posture in an occipito-transverse position. As the fetal head descends along the curve of Carus, passing P_2, P_3, and arriving at P_4, it rotates from the occipito-transverse position to the occipito-anterior position. The fetal head then keeps moving and is delivered at P_5.

4 Discussion

In this study, we have proposed an approach to obtain the curve of Carus for childbirth computational models with a fully prescribed descent trajectory during the second stage of labor. Three curves of Carus were obtained for a maternal pelvis with fetal heads of three different sizes (10th, 50th, and 90th percentile fetal head size at 37 weeks GA). This approach can be applied to any maternal pelvis and fetal head geometry combination in order to generate a fetal descent trajectory starting from the point of the fetal head engaging with the pelvic inlet to the point of the fetal head being fully delivered. A cubic spline interpolation method was used to obtain piece-wise polynomial coefficients for the entire trajectory. Compared to a one-piece polynomial interpolation, piece-wise spline interpolation effectively lowers the order of the polynomials and eliminates large oscillation between data points. By combining the position along the curve of Carus with rotational movements of the fetal head, cardinal movements of the fetal head were simulated in MADYMO.

Despite the fact that computational models have been widely used to explore a variety of childbirth-related topics, fetal descent trajectory as a crucial characteristic of labor still lacks well-rounded solutions and detailed procedure documentation. Some studies use a straight fetal descent trajectory as an approximation when the required displacements are relatively small. In a study investigating the deformation and stress distribution of the pelvic floor, Noritomi et al. [36] imposed straight movements on their spherical fetal head model. The trajectory started from the fetal head engaging the pelvic floor and ended before the fetal head's diameter passed the pelvic floor. In another study investigating pelvic floor deformation and stress, Berardi et al. [37] simulated a vertical translation of the spherical fetal head from where it engaged with the pelvic floor to its diameter passing the genital hiatus of the pelvic floor. In a series of studies [6,8,17,38,39] using the same computational modeling framework, Parente and colleagues imposed descent trajectories by applying displacements and rotations to several points on the fetal model. The same author group later updated the descent trajectory in this modeling framework by allowing an increased degree-of-freedom for the fetus [21–25,40]: vertical movements of the fetal model were controlled by the rigid reference point at the craniocervical junction,

Table 1 Measurements of the 10th, 50th, and 90th percentile sized fetal head at 37 weeks in the current study as well as fetal head measurements from other computational studies in the literature for comparison

	Fetal head measurements at 37 weeks in current study							
(Units: mm)	10th percentile	50th percentile	90th percentile	Lapeer and Prager [28]	Krofta et al. [27]	Oliveira et al. [46]	Martins et al. [6]	Parente et al. [33]
Biparietal	88.4	93.2	97.9	89.7	93.7	—	—	95.0
Occipito-frontal	109.7	117.5	125.2	119.7	105.7	115.0	120.0	115.0
Suboccipito-bregmatic	85.6	90.7	95.6	88.7	100.3	95.0	100.0	—
Orbito-occipital	—	—	—	119.9	—	—	—	—
Maxilla-vertical	—	—	—	129.3	—	—	—	—
Orbito-vertical	—	—	—	119.3	—	—	—	—
Suboccipito-frontal	—	—	—	113.2	—	105.0	105.0	105.0
Occipito-mental	—	—	—	—	131.9	—	—	—
Submento-bregmatic	—	—	—	—	—	95.0	115.0	95.0
Mentovertical	—	—	—	—	—	130.0	130.0	130.0

but the fetus was allowed to translate in the plane perpendicular to the prescribed vertical movements to adapt to constraints from the maternal pelvis and pelvic floor muscles. Similar approaches can be found in studies from another group of authors – Nielsen and colleagues defined the fetal descent trajectory by altering the vertical coordinates for the top nodes of the head [16,26,27,41–44], and rotation of the fetal head was allowed in some cases to achieve less resistance [26,27].

The practice of applying displacements and rotations to the fetal model directly in the above studies is essentially the same approach used in the current study. However, no details of the fetal movements were disclosed in these studies. The practice of applying vertical displacements in the descent direction while allowing translational and rotational freedom in other directions faces the same challenge as force-driven movements do: a high level of maternal soft tissue completeness is required for the fetal movements to be accurate since maternal soft tissues will bear the responsibility of defining the fetal descent trajectory. However maternal soft tissues in the studies mentioned above only included levator ani muscles. Fetal movements will lose constraints after the fetal head passes the levator ani, and therefore a full descent trajectory cannot be achieved.

There have been a few studies that have used the curve of Carus to prescribe fetal movements in computational studies. In two studies investigating levator ani muscle stretch [4] and pudendal nerve stretch [29] by Lien and colleagues, the curve of Carus was constructed by defining eight equally spaced locations between the point where the fetal head engages the iliococcygeal muscle and the point where the spherical fetal head's diameter passed the pubococcygeal muscle. In another two studies investigating manual perineal protection by Jansova et al. [14,15], and a study investigating levator ani muscle stress distribution by Krofta et al. [30], the curve of Carus was also used to define fetal model movements. Although no detailed procedure to derive the curve of Carus was offered in these studies, Jansova et al. [15] described the trajectory as "the head pivoted as closely as possible around the lower margin of the pubic symphysis", which agrees with the current study on the characteristics of the most important landmark point on the curve of Carus, namely, P_4.

We also identified two studies in the literature that used imaging data to define fetal movements in computational models. Hoyte et al. [7] used the path of the vagina obtained through MRI data to define the descent trajectory for the fetal model. Sindhwani et al. [45] captured the fetal head movements through the levator ani muscles during childbirth using real-time dynamic MRI in the midsagittal plane, and 3D deformational and translational fields of the fetal head were defined accordingly. Although the descent trajectories in these two studies are still relatively short (not passing

Table 2 Coordinates (x, z) of landmark points P_1 through P_5 on the curve of Carus for fetal heads of 10th, 50th, and 90th percentile sizes at 37 weeks. All points are in units of mm. P_1 through P_5 are all on the sagittal plane at $y = -1.9$ mm.

	P_1	P_2	P_3	P_4	P_5
10th	(−58.8, −20.6)	(−41.3, −55.6)	(−17.7, −70.2)	(41.3, −85.0)	(129.7, 3.4)
50th				(42.5, −88.2)	(130.9, 0.2)
90th				(43.8, −91.5)	(132.2, −3.1)

Table 3 Polynomial coefficients a, b, c, and d for each interval of the curve of Carus for fetal heads of 10th, 50th, and 90th percentile sizes at 37 weeks

		P_1P_2	P_2P_3	P_3P_4	P_4P_5
10th	a	-5.37×10^{-4}	-5.37×10^{-4}	4.66×10^{-5}	4.66×10^{-5}
	b	6.51×10^{-2}	3.69×10^{-2}	-1.13×10^{-3}	7.12×10^{-3}
	c	−2.97	−1.19	−0.35	6.80×10^{-3}
	d	−20.60	−55.60	−70.20	−85.00
50th	a	-5.52×10^{-4}	-5.52×10^{-4}	5.19×10^{-5}	5.19×10^{-5}
	b	6.60×10^{-2}	3.70×10^{-2}	-2.10×10^{-3}	7.28×10^{-3}
	c	−2.99	−1.18	−0.36	-4.91×10^{-2}
	d	−20.60	−55.60	−70.20	−88.20
90th	a	-5.66×10^{-4}	-5.66×10^{-4}	5.68×10^{-5}	5.68×10^{-5}
	b	6.68×10^{-2}	3.71×10^{-2}	-3.03×10^{-3}	7.45×10^{-3}
	c	−3.00	−1.18	−0.37	−0.10
	d	−20.60	−55.60	−70.20	−91.50

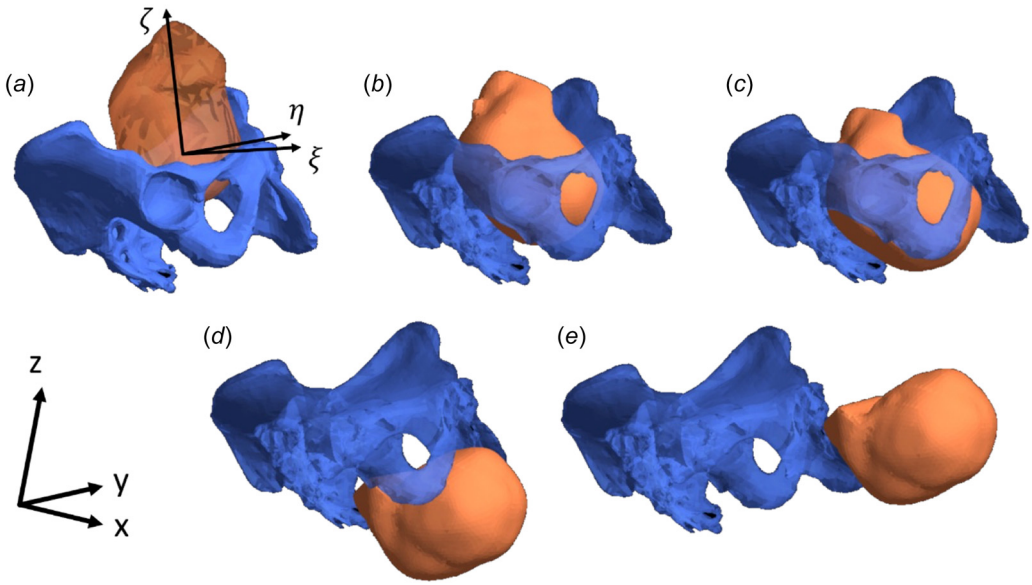

Fig. 4 Fetal head positions at each of the landmark points during childbirth are shown: (*a*) at P_1, (*b*) at P_2, (*c*) at P_3, (*d*) at P_4, and (*e*) at P_5 with fetal head being delivered. The fetal head local coordinate system is shown in (*a*), where ζ is the longitudinal axis and ξ is the transverse axis. The global coordinate system (x-y-z) is also marked. The fetal head in the picture is of the 50th percentile size at 37 weeks.

P_4), imaging data (especially imaging data of live births) could serve as valuable reference data to validate and improve the accuracy of generic descent trajectory models, like the one proposed in the current study.

In the literature, many of the descent trajectories in computational studies do not reach the pubic arch plane, P_4 in the current study. This could be due to the fact that levator ani muscle stretch during childbirth is the most studied topic in computational models, and modeling this topic does not require the entire second stage of labor to be simulated. The lack of maternal soft tissues other than the levator ani could further have limited the capability of these published computational models to simulate the entire curve of Carus, as soft tissue constraints would be required to guide the fetal models' movements. Lapeer et al. [20] did describe the position of the fetal head along the full delivery trajectory as well as rotation in both the sagittal and transverse planes, having developed a complex mathematical framework for a virtual reality simulation of childbirth. Within this simulation, intra-uterine expulsive forces were applied to move the fetus through the pelvis and soft tissue of the birth canal. Their simulation occurred over 216 s, and it exhibited the characteristic (and sequential) flexion, internal rotation, extension, and external rotation seen within the cardinal movements of labor. This elegant study, as a force-driven model using explicit FE methods within an entity-component

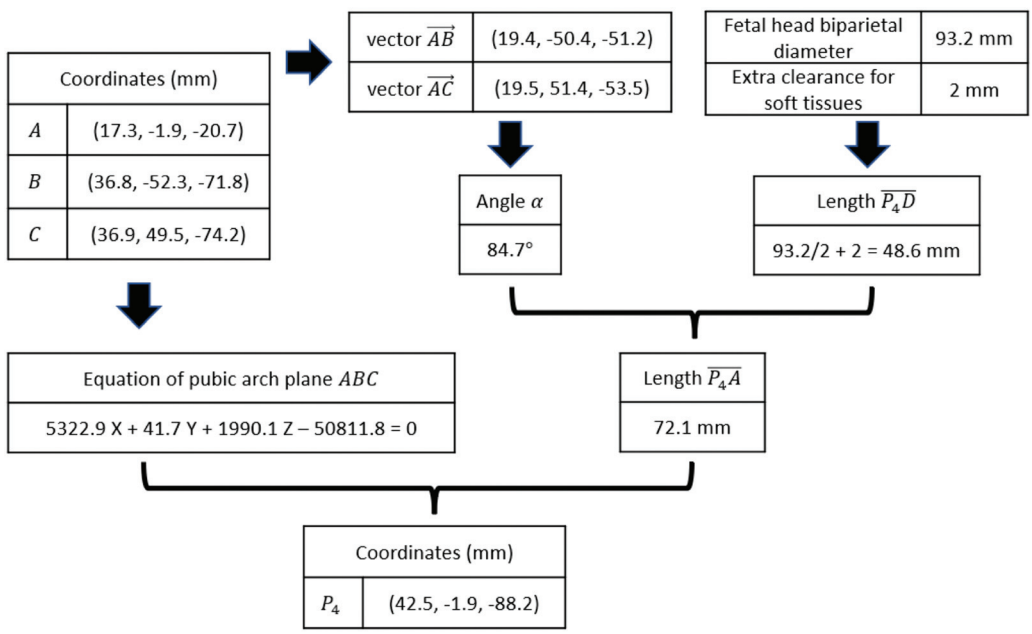

Fig. 5 The calculation of P_4 coordinates based on the geometric relationship between the maternal pubic arch plane and the fetal head size. A fetal head size of the 50th percentile at 37 weeks is used to obtain the values in this figure.

system, provides a virtual representation of the movement of the infant through the pelvis that the authors propose can be used for training purposes. It provides one tool with which to investigate the interaction of the fetus and the maternal tissue. Connection of Lapeer's simulation results with other current work on the modeling of both maternal and fetal responses during childbirth may bridge some of the challenges that exist when validating these models. However, the mathematical complexity of this virtual reality simulation supports the continued use of other, more traditional finite element models of the birth process—using either a displacement-controlled or force-controlled movement of the fetus—in order to address some of the fundamental questions that remain regarding the pathomechanics of maternal and fetal injury during vaginal birth.

The current study provides a universal approach to defining the curve of Carus in displacement-driven models of childbirth. The method can be applied to any shape and size of pelvis, as pelvic geometry guides the definition of points P1 through P4, either entirely or in part. Rotational movements of the fetal head are also integrated to simulate the cardinal movements. As a universal, numerical approach to defining a fetal descent trajectory, the movements of the fetal head in each of the planes are simplified compared to physiological labor. Firstly, the descent trajectory is unlikely to be a perfectly smooth curve, considering the irregular shapes of internal organs and other maternal soft tissues, let alone with a continuous first and second-order derivative. Secondly, the fetus does not actually move at a constant speed during the second stage of labor. Periodic uterine contraction along with voluntary maternal pushing generates discontinuous pressure to facilitate the fetal descent, which leads to the fetus moving at variable speeds. Thirdly, extension was not modeled in this study. We feel that, in order to provide the anatomical constraint to that motion, the inclusion of an articulated fetal neck within the model is important if extension is to be simulated. Extension is an important response to include when examining either maternal soft tissue response or fetal soft tissue response during the second stage of labor, but it is less relevant when demonstrating that the fetal head can follow the derived curve of Carus. Finally, as the soft tissue has not been included in this current examination of the curve of Carus, and the fetal model does not include the infant's body, restitution did not occur in this simulation. When the fetal head delivers at P_5, the restitution process should occur to return the head to a neutral position. Restitution occurs when the head clears the soft tissue of the perineum based on the head's natural movement, but it may require gentle clinician assistance – typically to a position that is more occiput transverse than occiput anterior. This rotation also helps the fetal head recover from the flexed "chin to the chest" position.

Despite the simplification of the curve of Carus in the current study, we have established a solid foundation for a computational modeling framework that included: (1) the curve of Carus with an exceptional length, ranging from the point of the fetal head engaging the pelvic inlet to the point of the fetal head being delivered; and (2) cardinal movements of the fetal head, namely, engagement, descent, flexion, and internal rotation. We also demonstrated that this approach can work regardless of the fetal head size. This modeling framework can be used to investigate a variety of childbirth-related topics on both the maternal and the fetal side and support comparison between different models.

Acknowledgment

The authors wish to thank Dr. Lapeer for sharing the 3D model of the fetal skull that he reported in his 2001 publication.

Funding Data

- National Science Foundation (Grant No. NSF 2028474 (CBET—DARE); Funder ID: 10.13039/100000001).

References

[1] Chaliha, C., 2009, "Postpartum Pelvic Floor Trauma," Curr. Opin. Obstet. Gynecol., **21**(6), pp. 474–479.
[2] Grimm, M. J., 2016, "Maternal Endogenous Forces and Shoulder Dystocia," Clin. Obstet. Gynecol., **59**(4), pp. 820–829.
[3] American College of Obstetricians and Gynecologists, ed., 2014, *Neonatal Brachial Plexus Palsy*, The American College of Obstetricians and Gynecologists, Women's Health Care Physicians, Washington, DC.
[4] Lien, K.-C., Mooney, B., DeLancey, J. O. L., and Ashton-Miller, J. A., 2004, "Levator Ani Muscle Stretch Induced by Simulated Vaginal Birth," Obstet. Gynecol., **103**(1), pp. 31–40.
[5] d'Aulignac, D., Martins, J. A. C., Pires, E. B., Mascarenhas, T., and Jorge, R. N., 2005, "A Shell Finite Element Model of the Pelvic Floor Muscles," Comput. Methods Biomech. Biomed. Eng., **8**(5), pp. 339–347.
[6] Martins, J. A. C., Pato, M. P. M., Pires, E. B., Jorge, R. M. N., Parente, M., and Mascarenhas, T., 2007, "Finite Element Studies of the Deformation of the Pelvic Floor," Ann. New York Acad. Sci., **1101**(1), pp. 316–334.
[7] Hoyte, L., Damaser, M. S., Warfield, S. K., Chukkapalli, G., Majumdar, A., Choi, D. J., Trivedi, A., and Krysl, P., 2008, "Quantity and Distribution of Levator Ani Stretch During Simulated Vaginal Childbirth," Am. J. Obstet. Gynecol., **199**(2), pp. 198.e1–198-e5.
[8] Parente, M. P. L., Jorge, R. M. N., Mascarenhas, T., Fernandes, A. A., and Martins, J. A. C., 2007, "Deformation of the Pelvic Floor Muscles During a Vaginal Delivery," Int. Urogynecol. J., **19**(1), pp. 65–71.
[9] Hage-Fransen, M. A. H., Wiezer, M., Otto, A., Wieffer-Platvoet, M. S., Slotman, M. H., der Sanden, M. W. G. N., and Pool-Goudzwaard, A. L., 2021, "Pregnancy- and Obstetric-Related Risk Factors for Urinary Incontinence, Fecal Incontinence, or Pelvic Organ Prolapse Later in Life: A Systematic Review and Meta-Analysis," Acta Obstet. Gynecol. Scand., **100**(3), pp. 373–382.
[10] Lapeer, R., Audinis, V., Gerikhanov, Z., and Dupuis, O., 2014, "A Computer-Based Simulation of Obstetric Forceps Placement," *Medical Image Computing and Computer-Assisted Intervention – MICCAI 2014*, P. Golland, N. Hata, C. Barillot, J. Hornegger, and R. Howe, eds., Springer International Publishing, Cham, pp. 57–64.
[11] Lapeer, R., Gerikhanov, Z., and Audinis, V., 2014, "A Computer-Based Simulation of Vacuum Extraction During Childbirth," SIMULIA Regional User Meeting RUM 2014, Warrington, UK, Nov. 4–5.
[12] Gonik, B., Zhang, N., and Grimm, M. J., 2003, "Prediction of Brachial Plexus Stretching During Shoulder Dystocia Using a Computer Simulation Model," Am. J. Obstet. Gynecol., **189**(4), pp. 1168–1172.
[13] Grimm, M. J., Costello, R. E., and Gonik, B., 2010, "Effect of Clinician-Applied Maneuvers on Brachial Plexus Stretch During a Shoulder Dystocia Event: Investigation Using a Computer Simulation Model," Am. J. Obstet. Gynecol., **203**(4), pp. 339.e1–339.e5.
[14] Jansova, M., Kalis, V., Rusavy, Z., Zemcik, R., Lobovsky, L., and Laine, K., 2014, "Modeling Manual Perineal Protection During Vaginal Delivery," Int. Urogynecol. J., **25**(1), pp. 65–71.
[15] Jansova, M., Kalis, V., Rusavy, Z., Räisänen, S., Lobovsky, L., and Laine, K., 2017, "Fetal Head Size and Effect of Manual Perineal Protection," Plos One, **12**(12), p. e0189842.
[16] Li, X., Kruger, J. A., Chung, J.-H., Nash, M. P., and Nielsen, P. M. F., 2008, "Modelling Childbirth: Comparing Athlete and Non-Athlete Pelvic Floor Mechanics," *Medical Image Computing and Computer-Assisted Intervention – MICCAI 2008*, D. Metaxas, L. Axel, G. Fichtinger, and G. Székely, eds., Springer, Berlin, Heidelberg, pp. 750–757.
[17] Parente, M. P., Natal Jorge, R. M., Mascarenhas, T., Fernandes, A. A., and Silva-Filho, A. L., 2010, "Computational Modeling Approach to Study the Effects of Fetal Head Flexion During Vaginal Delivery," Am. J. Obstet. Gynecol., **203**(3), pp. 217.e1–217.e6.
[18] Buttin, R., Zara, F., Shariat, B., and Redarce, T., 2009, "A Biomechanical Model of the Female Reproductive System and the Fetus for the Realization of a Childbirth Virtual Simulator," Annual International Conference of the IEEE Engineering in Medicine and Biology Society, Minneapolis, MN, Sept. 2–6, pp. 5263–5266.
[19] Buttin, R., Zara, F., Shariat, B., Redarce, T., and Grangé, G., 2013, "Biomechanical Simulation of the Fetal Descent Without Imposed Theoretical Trajectory," Comput. Methods Prog. Biomed., **111**(2), pp. 389–401.
[20] Lapeer, R., Gerikhanov, Z., Sadulaev, S.-M., Audinis, V., Rowland, R., Crozier, K., and Morris, E., 2019, "A Computer-Based Simulation of Childbirth Using the Partial Dirichlet–Neumann Contact Method With Total Lagrangian Explicit Dynamics on the GPU," Biomech. Model Mechanobiol., **18**(3), pp. 681–700.
[21] Silva, M. E. T., Oliveira, D. A., Roza, T. H., Brandão, S., Parente, M. P. L., Mascarenhas, T., and Natal Jorge, R. M., 2015, "Study on the Influence of the Fetus Head Molding on the Biomechanical Behavior of the Pelvic Floor Muscles, During Vaginal Delivery," J. Biomech., **48**(9), pp. 1600–1605.
[22] Oliveira, D. A., Parente, M. P. L., Calvo, B., Mascarenhas, T., and Jorge, R. M. N., 2016, "A Biomechanical Analysis on the Impact of Episiotomy During Childbirth," Biomech Model Mechanobiol., **15**(6), pp. 1523–1534.
[23] Oliveira, D. A., Parente, M. P. L., Calvo, B., Mascarenhas, T., and Jorge, R. M. N., 2017, "The Management of Episiotomy Technique and Its Effect on Pelvic Floor Muscles During a Malposition Childbirth," Comput. Methods Biomech. Biomed. Eng., **20**(11), pp. 1249–1259.
[24] Vila Pouca, M. C. P., Ferreira, J. P. S., Oliveira, D. A., Parente, M. P. L., Mascarenhas, T., and Natal Jorge, R. M., 2018, "On the Effect of Labour Durations

Using an Anisotropic Visco-Hyperelastic-Damage Approach to Simulate Vaginal Deliveries," J. Mech. Behav. Biomed. Mater., **88**, pp. 120–126.
[25] Pouca, M. C. P. V., Ferreira, J. P. S., Oliveira, D. A., Parente, M. P. L., and Jorge, R. M. N., 2018, "Viscous Effects in Pelvic Floor Muscles During Childbirth: A Numerical Study," Int. J. Numer. Methods Biomed. Eng., **34**(3), p. e2927.
[26] Li, X., Kruger, J. A., Nash, M. P., and Nielsen, P. M. F., 2010, "Effects of Nonlinear Muscle Elasticity on Pelvic Floor Mechanics During Vaginal Childbirth," ASME J. Biomech. Eng., **132**(11), p. 111010.
[27] Yan, X., Kruger, J. A., Nash, M. P., and Nielsen, P. M. F., 2012, "Effects of Levator Ani Muscle Morphology on the Mechanics of Vaginal Childbirth," *Computational Biomechanics for Medicine*, P. M. F. Nielsen, A. Wittek, and K. Miller, eds., Springer, New York, pp. 63–75.
[28] Routzong, M. R., Moalli, P. A., Maiti, S., De Vita, R., and Abramowitch, S. D., 2019, "Novel Simulations to Determine the Impact of Superficial Perineal Structures on Vaginal Delivery," Interface Focus, **9**(4), p. 20190011.
[29] Lien, K.-C., Morgan, D. M., Delancey, J. O. L., and Ashton-Miller, J. A., 2005, "Pudendal Nerve Stretch During Vaginal Birth: A 3D Computer Simulation," Am. J. Obstet. Gynecol., **192**(5), pp. 1669–1676.
[30] Krofta, L., Havelková, L., Urbánková, I., Krčmář, M., Hynčík, L., and Feyereisl, J., 2017, "Finite Element Model Focused on Stress Distribution in the Levator Ani Muscle During Vaginal Delivery," Int. Urogynecol. J., **28**(2), pp. 275–284.
[31] Carus, C. G., 1820, *Lehrbuch Der Gynäkologie*, Bd. 1., Fleischer, Leipzig, Germany.
[32] Grimm, M. J., 2021, "Forces Involved With Labor and Delivery-A Biomechanical Perspective," Ann. Biomed. Eng., **49**(8), pp. 1819–1835.
[33] Lapeer, R. J., and Prager, R. W., 2001, "Fetal Head Moulding: Finite Element Analysis of a Fetal Skull Subjected to Uterine Pressures During the First Stage of Labour," J. Biomech., **34**(9), pp. 1125–1133.
[34] Chitty, L. S., Altman, D. G., Henderson, A., and Campbell, S., 1994, "Charts of Fetal Size: 2. Head Measurements*," BJOG: An Int. J. Obstet. Gynaecol., **101**(1), pp. 35–43.
[35] Malas, M. A., Üngör, B., Tağıl, S. M., and Sulak, O., 2006, "Determination of Dimensions and Angles of Mandible in the Fetal Period," Surg. Radiol. Anat., **28**(4), pp. 364–371.
[36] Noritomi, P. Y., J. V. Lopes, d S., Dellai, R. C. A., Fiorentino, A., Giorleo, L., and Ceretti, E., 2013, "Virtual Modeling of a Female Pelvic Floor and Hypothesis for Simulating Biomechanical Behavior During Natural Delivery," Procedia CIRP, **5**, pp. 300–304.
[37] Berardi, M., Martinez-Romero, O., Elías-Zúñiga, A., Rodríguez, M., Ceretti, E., Fiorentino, A., Donzella, G., and Avanzini, A., 2014, "Levator Ani Deformation During the Second Stage of Labour," Proc. Inst. Mech. Eng. H, **228**(5), pp. 501–508.
[38] Parente, M. P., Natal Jorge, R. M., Mascarenhas, T., and Silva-Filho, A. L., 2010, "The Influence of Pelvic Muscle Activation During Vaginal Delivery," Obstet. Gynecol., **115**(4), pp. 804–808.
[39] Parente, M. P. L., Jorge, R. M. N., Mascarenhas, T., Fernandes, A. A., and Martins, J. A. C., 2009, "The Influence of an Occipito-Posterior Malposition on the Biomechanical Behavior of the Pelvic Floor," Eur. J. Obstet. Gynecol. Reprod. Biol., **144**, pp. S166–S169.
[40] Oliveira, D. A., Parente, M. P. L., Calvo, B., Mascarenhas, T., and Natal Jorge, R. M., 2016, "Numerical Simulation of the Damage Evolution in the Pelvic Floor Muscles During Childbirth," J. Biomech., **49**(4), pp. 594–601.
[41] Yan, X., Kruger, J. A., Nielsen, P. M. F., and Nash, M. P., 2015, "Effects of Fetal Head Shape Variation on the Second Stage of Labour," J. Biomech., **48**(9), pp. 1593–1599.
[42] Li, X., Kruger, J. A., Nash, M. P., and Nielsen, P. M. F., 2011, "Anisotropic Effects of the Levator Ani Muscle During Childbirth," Biomech. Model Mechanobiol., **10**(4), pp. 485–494.
[43] Mayeur, O., Jeanditgautier, E., Witz, J.-F., Lecomte-Grosbras, P., Cosson, M., Rubod, C., and Brieu, M., 2017, "Evaluation of Strains on Levator Ani Muscle: Damage Induced During Delivery for a Prediction of Patient Risks," *Computational Biomechanics for Medicine*, A. Wittek, G. Joldes, P.M.F. Nielsen, B.J. Doyle, and K. Miller, eds., Springer International Publishing, Cham, pp. 135–146.
[44] Li, X., Kruger, J. A., Chung, J.-H., Nash, M. P., and Nielsen, P. M. F., 2008, "Modelling the Pelvic Floor for Investigating Difficulties During Childbirth," Medical Imaging 2008: Physiology, Function, and Structure From Medical Images, International Society for Optics and Photonics, San Diego, CA, Feb. 17–19, p. 69160V.
[45] Sindhwani, N., Bamberg, C., Famaey, N., Callewaert, G., Dudenhausen, J. W., Teichgräber, U., and Deprest, J., 2017, "In Vivo Evidence of Significant Levator Ani Muscle Stretch on MR Images of a Live Childbirth," Am. J. Obstet. Gynecol., **217**(2), pp. 194.e1–194.e8.
[46] Oliveira, D., Pouca, M. V., Ferreira, J., and Mascarenhas, T., 2019, "Episiotomy: The Biomechanical Impact of Multiple Small Incisions During a Normal Vaginal Delivery," Interface Focus, **9**(5), p. 20190027.